The Ozone Hole Breakup in September 2002 as Seen by SCIAMACHY on *ENVISAT*

C. VON SAVIGNY, A. ROZANOV, H. BOVENSMANN, K.-U. EICHMANN, S. NOËL, V. V. ROZANOV,
B.-M. SINNHUBER, M. WEBER, AND J. P. BURROWS

Institute of Environmental Physics, University of Bremen, Bremen, Germany

J. W. KAISER

Remote Sensing Laboratories, University of Zurich, Zurich, Switzerland

ABSTRACT

An unprecedented stratospheric warming in the Southern Hemisphere in September 2002 led to the breakup of the Antarctic ozone hole into two parts. The Scanning Imaging Absorption Spectrometer for Atmospheric Chartography (SCIAMACHY) on the European *Environmental Satellite* (*ENVISAT*) performed continuous observations of limb-scattered solar radiance spectra throughout the stratospheric warming. Thereby, global measurements of vertical profiles of several important minor constituents are provided with a vertical resolution of about 3 km. In this study, stratospheric profiles of O_3, NO_2, and BrO retrieved from SCIAMACHY limb-scattering observations together with polar stratospheric cloud (PSC) observations for selected days prior to (12 September), during (27 September), and after (2 October) the ozone hole split are employed to provide a picture of the temporal evolution of the Antarctic stratosphere's three-dimensional structure.

1. Introduction

The temporal evolution of the Southern Hemisphere polar stratosphere during September 2002 was characterized by the occurrence of an unprecedented major stratospheric warming (Allen et al. 2003; Baldwin et al. 2003; Hoppel et al. 2003; Newman and Nash 2005; Sinnhuber et al. 2003; Varotsos 2003; Weber et al. 2003). These warmings are common in the Northern Hemisphere but have not been observed before in the Southern Hemisphere (Baldwin et al. 2003; Sinnhuber et al. 2003). The enhanced planetary wave activity that caused the major warming significantly affected the Antarctic ozone hole. The ozone hole was markedly smaller than in previous years and according to Stolarski et al. (2005), the area within the 220 DU contour [1 DU (Dobson unit) = 2.89×10^{16} molecules cm^{-2}]—commonly used for the definition of the ozone hole—was only about 10% of its usual size. Moreover, the ozone hole split into two parts after 22 September 2002. Such a splitting of the Antarctic ozone hole and polar vortex has also not been observed before (Roscoe et al. 2005).

Several studies have already pointed out that the comparatively large total ozone columns over Antarctica after the ozone hole split are mainly a consequence of the unusual dynamical conditions and not primarily caused by reduced chemical ozone destruction (e.g., Hoppel et al. 2003; Newman and Nash 2005; Sinnhuber et al. 2003). Hoppel et al. (2003) report nominal ozone loss until the occurrence of the major stratospheric warming but found reduced ozone loss after the warming. This is most likely a consequence of the disappearance of polar stratospheric clouds (PSCs) due to increased temperatures. The overall chemical ozone loss in the 14–20-km range was found to be only about 20% smaller than in previous years (Hoppel et al. 2003). This is consistent with the finding by Sinnhuber et al. (2003) that the estimated chemical ozone loss south of 63° is only slightly lower than in previous years.

Total ozone column measurements during the anomalous evolution of the 2002 Antarctic ozone hole were performed by the National Aeronautics and Space Administration/National Oceanic and Atmospheric Adminstration (NASA/NOAA) Total Ozone Mapping Spectrometer (TOMS) on the Earth Probe platform (Stolarski et al. 2005) and by the Global Ozone Monitoring Experiment (GOME) on the second European Remote Sensing satellite, *ERS-2* (Sinnhuber et al. 2003; Weber et al. 2003). These measurements yield essential information for the understanding of the ozone hole split, but they do not provide information on the verti-

Corresponding author address: Dr. Christian von Savigny, Institute of Environmental Physics, University of Bremen, Otto-Hahn-Alle 1, 28334 Bremen, Germany.
E-mail: csavigny@iup.physik.uni-bremen.de

cal structure of the atmosphere during the event. A novel remote sensing technique allowing daily near-global measurements of the atmospheric composition from space with high vertical resolution (2–3 km) employs spectrally resolved limb measurements of the solar radiation scattered in the earth's atmosphere (Flittner et al. 2000; McPeters et al. 2000; Sioris et al. 2003; von Savigny et al. 2003). One of the few instruments capable of performing measurements of limb-scattered solar radiation from space is the Scanning Imaging Absorption Spectrometer for Atmospheric Chartography (SCIAMACHY; Bovensmann et al. 1999), which continuously monitored the stratosphere on the sunlit side of the globe throughout the duration of the major stratospheric warming and the subsequent ozone hole split.

The purpose of this paper is to describe the evolution of the anomalous development of the 2002 ozone hole based on SCIAMACHY observations of stratospheric O_3, NO_2, BrO, and PSCs.

The paper is structured as follows. Section 2 provides a brief overview of the SCIAMACHY instrument. In section 3, a summary of the methods used to retrieve minor constituent profiles from limb-scattering observations is presented. Results of SCIAMACHY observations of stratospheric O_3, NO_2, and BrO, as well as PSC observations, are presented in section 4. Three days are chosen for an in-depth study, namely, (i) 12 September, prior to the occurrence of the major stratospheric warming, (ii) 27 September, a few days after the ozone hole split, and (iii) 2 October, when one part of the polar vortex regained strength and was migrating back to the pole while the second fragment of the polar vortex and the ozone hole had almost disappeared into the midlatitudes. In section 5, the results are discussed and interpreted. It must be pointed out that the retrieval results will only be used in a qualitative manner since the SCIAMACHY scientific data products are only partly validated and due to the remaining limb-pointing issues (see section 2).

2. Instrumental description

SCIAMACHY is one of ten scientific instruments on board the European Space Agency's (ESA's) *Environmental Satellite* (*ENVISAT*), which was launched on 1 March 2002 from Kourou, French Guyana, into a sun-synchronous polar orbit with an inclination of 97.8° and a descending node at 1030 local solar time (LST). SCIAMACHY is the first instrument capable of performing spectroscopic observations of the earth's atmosphere in nadir-viewing mode and limb-viewing mode, as well as the solar and lunar occultation modes. For this study, only SCIAMACHY limb observations were employed. The novel limb-scattering method combines almost global coverage on a daily basis with high vertical resolution. More traditional UV/visible remote

sensing instruments for atmospheric composition measurements such as nadir-viewing spectrometers (e.g., TOMS) McPeters et al. 1998) and GOME (Burrows et al. 1999) or solar occultation instruments [e.g., the Stratospheric Aerosol and Gas Experiment (SAGE); McCormick et al. 1989] and Polar Ozone and Aerosol Measurement (POAM) series (Lucke et al. 1999) can only provide either global coverage (TOMS and GOME) or high vertical resolution (POAM and SAGE). SCIAMACHY consists of eight channels—each comprised of a grating—covering the spectral range between 220 nm and 2.4 μm with a wavelength-dependent spectral resolution of 0.1–1.5 nm. In limb observation mode the earth's limb is stepped through for a tangent height (TH) range between about −3 and 100 km in steps of about 3.3 km. After each TH step an azimuthal scan is performed, covering a distance of about 960 km at the tangent point (TP). SCIAMACHY's instantaneous field of view (IFOV) is 2.6 km vertically and 110 km horizontally at the TP. Further information on the SCIAMACHY instrument and its mission objectives are provided in Bovensmann et al. (1999).

It must be noted that problems with the limb pointing were experienced since the start of the mission and have not been fully resolved as of yet. Evidence of pointing errors comes from different sources: (i) altitude offsets between SCIAMACHY O_3 and NO_2 density profiles and profiles measured with independent methods (Bracher et al. 2003) and (ii) tangent height retrievals from the limb radiance measurements themselves, by exploiting the "knee," that is, a maximum in the UV limb radiance profiles due to absorption of solar radiation in the Huggins and Hartley bands of ozone (Sioris et al. 2001; Kaiser et al. 2004, manuscript submitted to *Can. J. Phys.*). The tangent height retrievals indicated that the limb pointing is very accurate immediately after updates of the onboard orbit model that occur twice a day. Between these updates, when the satellite position is solely determined by the orbit propagator model, SCIAMACHY's limb pointing starts to deviate from nominal pointing until the next orbit model update takes place. Pointing errors of up to about 60 mdeg were found to occur, translating to tangent height offsets of about 3 km. These findings are consistent in terms of sign, magnitude, and temporal behavior with the pointing offsets of the Michelson Interferometer for Passive Atmospheric Sounding (MIPAS; von Clarmann et al. 2003), another limb viewing instrument aboard *ENVISAT* (Fischer and Oelhaf 1996). In conclusion, both (i) the consistency between SCIAMACHY and MIPAS pointing errors and (ii) the dependence on the onboard orbit model updates strongly indicate that the pointing errors originate from an incorrect knowledge of the orientation/position of the satellite platform and are not due to the individual instruments.

As a first-order pointing correction, a constant offset of 1.5 km was subtracted from the engineering THs

provided in the data files prior to the retrievals for all results presented here. It must be noted that with this correction and the greatest expected TH errors of 3 km, errors of up to 1.5 km may still occur. Therefore, the analysis presented here is limited to a qualitative rather than a quantitative description of the Antarctic vortex split in September 2002.

3. Methodology

a. Ozone profile retrievals

The ozone profile retrieval method employed here follows the method developed to retrieve stratospheric ozone density profiles from limb-scattering measurements performed with the Shuttle Ozone Limb Sounding Experiment/Limb Ozone Retrieval Experiment (SOLSE/LORE; McPeters et al. 2000; Flittner et al. 2000), two limb-viewing spectrometers flown on NASA's space shuttle mission STS-87 in 1997. A similar approach is also applied for operational ozone profile retrievals (von Savigny et al. 2003; Petelina et al. 2004) from limb-scattering measurements with the Optical Spectrograph and Infrared Imager System (OSIRIS; Llewellyn et al. 1997) instrument on the Swedish-led Odin satellite. The method exploits the differential absorption between the center ($\lambda_1 = 600$ nm) and the wings ($\lambda_2 = 525$ nm/$\lambda_3 = 675$ nm) of the Chappuis absorption bands ($^1B_1 \leftarrow X^1A_1$) of ozone. Limb radiance profiles $I(\lambda, \text{TH})$ at these wavelengths are normalized with respect to a reference TH of $\text{TH}_{\text{ref}} = 43$ km: $I_N(\lambda, \text{TH}) = I(\lambda, \text{TH})/I(\lambda, \text{TH}_{\text{ref}})$. The normalized limb radiance profiles are then combined to the *Chappuis retrieval vector,*

$$\mathbf{y}(\text{TH}) = \frac{I_N(\lambda_1, \text{TH})}{\sqrt{I_N(\lambda_2, \text{TH}) \times I_N(\lambda_3, \text{TH})}}, \quad (1)$$

which is fed into a nonlinear Newtonian iteration version of optimal estimation (OE; Rodgers 1976) driving the spherical radiative transfer (RT) model, SCIARAYS (Kaiser 2002; Kaiser and Burrows 2003). SCIARAYS is not a full multiple scattering (MS) model, but takes two scattering orders into account. Yet, it was found that, even with a single scattering (SS) model, the retrieval errors are less than 2% at and above the ozone density peak altitudes. Below the ozone density peak the relative retrieval errors are bigger, but the absolute retrieval errors were found to be always lower then 2×10^{11} cm^{-3}. Since the contribution to the total limb radiance from the third and higher scattering orders is small compared to the first two orders, using only two scattering orders will result in retrieval errors of a few percent at the most within the 15–35-km altitude range. The altitude range between about 15 and 35–40 km is accessible with this technique. Below 15 km the line of sight optical depth becomes so large that these altitudes cannot be "seen" from space

in limb geometry, and above 35–40 km the absorption in the Chappuis bands becomes too weak.

Preliminary validation results indicate that the retrieved ozone profiles agree to within about 10%–15% with the Halogen Occultation Experiment (HALOE) and SAGE II within the 15–35-km altitude range (Bracher et al. 2002; Bracher et al. 2003). A more systematic validation, particularly under ozone hole conditions, is underway but is not yet finished.

b. NO$_2$ and BrO profile retrievals

Measurements of the scattered solar radiation in limb-viewing geometry as performed by the SCIAMACHY instrument are simulated using the combined differential-integral approach (CDI) radiative transfer model (Rozanov et al. 2001). The model calculates the limb radiance properly considering the single scattered radiance and using an approximation to account for multiple scattering.

The CDI radiative transfer model is linearized with respect to the absorption coefficient; that is, it can be used to calculate weighting functions of atmospheric trace gases needed by the retrieval procedure to evaluate the vertical distributions. The weighting function at a particular wavelength λ is defined as the change in the measured radiation at this wavelength, $I(\lambda)$, due to a change in the vertical profile of the trace gas of interest, α, at a certain altitude level z_i:

$$W_i(\lambda) = \frac{\delta I(\lambda)}{\delta \alpha_i} \alpha_i. \quad (2)$$

The retrieval is performed using ratios of limb spectra in a selected tangent height region to a limb measurement at a reference tangent height. For the BrO profile retrievals a reference tangent height of about 34 km is used; for NO$_2$ profile retrievals, it is about 46 km. The algorithm consists of two steps, namely, preprocessing aimed at getting rid of spectral features not associated to retrieved parameters and the main inversion procedure.

At the preprocessing step, the ratios of limb spectra at different tangent heights to the measurement at a reference tangent height are treated independently one by one. At each tangent height, in order to account for the broadband scattering characteristics of the atmosphere and broadband instrumental features, a polynomial of an appropriate order (third order for NO$_2$ and fifth order for BrO) is subtracted from the logarithms (i) of the measured limb radiance at this tangent height, (ii) of the measured limb radiance at the reference tangent height (reference spectrum), and (iii) of the simulated ratio spectrum (i.e., ratio of modeled limb spectra at current and reference tangent heights) as well as from the logarithmic weighting functions. The resulting differential spectra $\tilde{I}_j^m$, $\tilde{I}_{\text{ref}}^m$, and R_j^s (i.e., measured, measured at the reference tangent height, and simulated, respectively) and differential weighting functions $\hat{W}$ are then given by

$$R_j^s = \ln\left[\frac{I_j^s(\lambda)}{I_{\text{ref}}^s(\lambda)}\right] - \sum_{i=0}^{N} a_{ij}^s \lambda^i,$$

$$\tilde{I}_{\text{ref}}^m = \ln[I_{\text{ref}}^m(\lambda)] - \sum_{i=0}^{N} a_{i,\text{ref}}^m \lambda^i \tag{3}$$

$$\hat{W}_j^k = \frac{1}{I_j^s(\lambda)} W_j^k(\lambda) - \frac{1}{I_{\text{ref}}^s(\lambda)} W_{\text{ref}}^k(\lambda) - \sum_{i=0}^{N} a_{ij}^k \lambda^i. \tag{4}$$

Here j denotes the tangent height index, k a retrieval parameter index, and N is a polynomial order. The weighting functions employed here are vertically integrated; that is, they represent a change of the differential limb radiance due to a scaling of a trace gas vertical profile.

Further in the course of the preprocessing step, a shift and squeeze correction as well as scaling factors for available correction spectra (e.g., ring spectrum, undersampling, stray light, etc.) are determined by minimizing the following quadratic form for each tangent height:

$$\left\| R_j^s(\lambda) + \sum_k W_j^k(\lambda) \frac{\Delta\alpha^k}{\alpha^k} - \tilde{I}_j^m(\lambda) + \tilde{I}_{\text{ref}}^m(\lambda) \right.$$

$$- \sum_l c_{\text{sc}}^l S_l(\lambda) - (c_{\text{shi}}^s - c_{\text{sq}}^s \lambda) \frac{\delta R_j^s(\lambda)}{\delta\lambda}$$

$$\left. - (c_{\text{shi}}^{\text{ref}} - c_{\text{sq}}^{\text{ref}} \lambda) \frac{\delta \tilde{I}_j^{\text{ref}}(\lambda)}{\delta\lambda} \right\|^2 \to \min. \tag{5}$$

Here c_{sc}^l are scaling factors for the correction spectra, $S_l(\lambda)$. The shift and squeeze correction is done for the ratio of modeled spectra with respect to the measured spectrum, represented by the coefficients c_{shi}^s and c_{sq}^s (index j omitted for simplicity) as well as for the limb measurement at the reference tangent height with respect to the measurement at current tangent height, represented by $c_{\text{shi}}^{\text{ref}}$ and $c_{\text{sq}}^{\text{ref}}$ (index j omitted for simplicity). In terms of the Ring effect correction the ratio of two Ring spectra at different tangent heights is simulated using the method described in Vountas et al. (1998), adapted for limb geometry for a standard atmosphere and then included in the fit procedure in the preprocessing step.

At the inversion step, vertical profiles of atmospheric trace gases are retrieved solving the following equation:

$$\mathbf{y} = \mathbf{K}\mathbf{x} + \boldsymbol{\varepsilon}. \tag{6}$$

Here, the measurement vector, **y**, contains the differences between ratios of simulated and measured differential limb spectra at all tangent heights with all corrections from the preprocessing step applied; the state vector, **x**, contains relative differences (with respect to the initial profiles) of trace gas number densities at all altitude layers for all gases to be retrieved. The linearized forward model operator, **K**, contains the corre-

sponding differential weighting functions, *W*. Equation (6) is solved employing the optimal estimation method (Rodgers 1990) for the BrO retrievals and the information operator approach (Hoogen et al. 1999) for the NO_2 retrievals.

The retrieval scheme applied here to stratospheric NO_2 and BrO profile retrievals does not involve the determination of absorber slant column densities [like, e.g., stratospheric trace gas retrievals from OSIRIS limb-scattering observations (Sioris et al. 2003; Haley et al. 2003)] as an intermediate data product. Instead, the retrieval algorithm directly minimizes the differences between the differential spectra derived from the RT calculations and from the measurements.

Stratospheric NO_2 profiles can be retrieved for the altitude range from about 15 up to 35–40 km. Besides shift and squeeze, only a stray light correction is done for NO_2 at the preprocessing step. The accuracy in retrieved number densities is estimated to be about 15%–20% between 15 and 30 km. Above, and for situations with little stratospheric NO_2, larger errors may occur. Further examples of NO_2 profile retrievals and preliminary validation results can be found in Eichmann et al. (2003) and Bracher et al. (2003). In terms of BrO the altitude coverage ranges from approximately 14–15 km to about 30 km. In addition to shift and squeeze correction, a differential ring spectrum (i.e., ratio of simulated ring spectra with a polynomial subtracted) is used at the preprocessing step for BrO. The retrieval accuracy is estimated to be about 30%–50%. First comparisons with balloonborne Differential Optical Absorption Spectroscopy (DOAS) solar occultation as well as balloonborne in situ (TRIPLE) measurements are consistent with this estimate (K. Pfeilsticker 2003, personal communication; F. Stroh 2003, personal communication; Dorf et al. 2004, manuscript submitted to *Atmos. Chem. Phys.*).

In Figs. 1 and 2 examples of NO_2 and BrO spectral fits and residuals are shown for the limb measurement at a latitude of 68°S and a longitude of 30°E of orbit 3008 (27 September 2002) at a TH of 19 km. Note that the residuals are more or less the same in the presence of larger O_3 abundances.

c. Detection of polar stratospheric clouds

Polar stratospheric clouds act as additional scatterers and therefore affect the observed limb radiance profiles. The color ratio

$$R_c(\text{TH}) = \frac{I(1090 \text{ nm, TH})}{I(750 \text{ nm, TH})}$$

is used for the detection of PSCs in a similar manner as for UV and visible wavelengths with ground-based spectrometers (e.g., Sarkissian et al. 1994). The wavelengths were chosen because they fall within weakly absorbing spectral intervals: 750 nm is between an H_2O absorption band centered at around 725 nm and the O_2
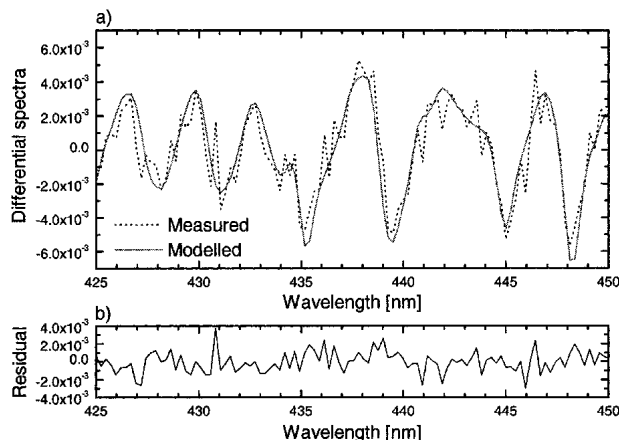
FIG. 1. Sample NO_2 spectral fit for the limb measurement at 68°S, 30°E during orbit 3008 (27 Sep 2002) at a TH of 19 km. The standard deviation of the residual is 1.13×10^{-3}.

FIG. 3. Color ratios $I(1090 \text{ nm})/I(750 \text{ nm})$ for several limb measurements during orbit 02796 on 12 Sep 2002.

A band ($b^1\Sigma_g^+ \rightarrow X^3\Sigma_g^-$) starting at 758 nm; 1090 nm falls between two H_2O bands centered at around 940 and 1130 nm. Figure 3 shows examples of color ratio profiles observed in the Southern Hemisphere part of orbit 2796 on 12 September 2002. Cases a and b are equatorward of the regime where lower-stratospheric temperatures are low enough for PSCs to be formed. Yet, an enhancement of the color index below about 30 km is discernible that is due to stratospheric sulphate aerosols. At 47°S (case b), this enhancement occurs at a lower TH, as expected. In cases c and d, strongly enhanced color ratios below 25 km occur due to the presence of PSCs.

Simulations with the radiative transfer model LIMBTRAN (Griffioen and Oikarinen 2000) were performed for the SCIAMACHY limb-viewing geometry at high southern latitudes to determine theoretical gradients—that is, $R_c(TH)/R_c(TH + \Delta TH)$, where $\Delta TH = 3.3$ km is the tangent height step size of the
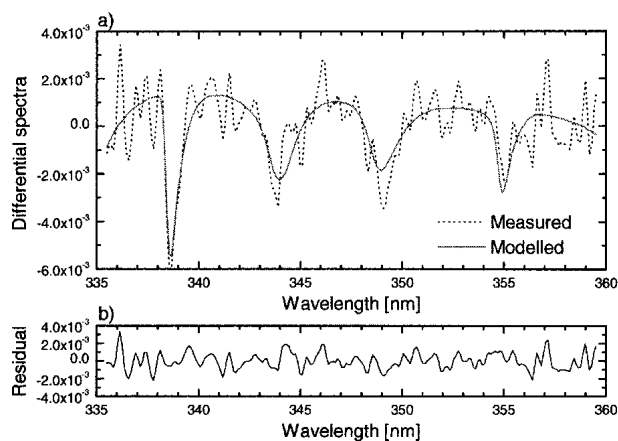

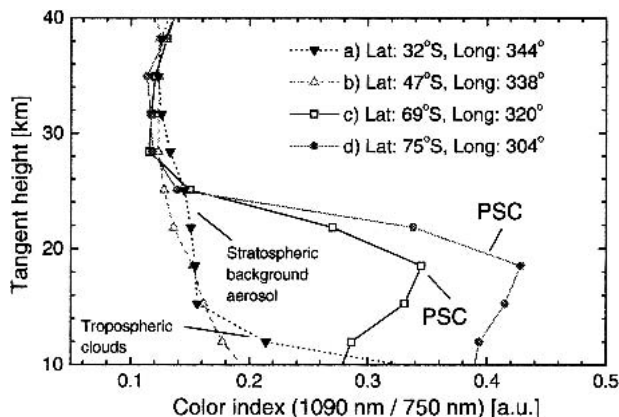FIG. 2. As in Fig. 1 but for BrO. The standard deviation of the residual is 9.22×10^{-4}.

SCIAMACHY limb observations—of the color ratio profiles for (i) a pure Rayleigh atmosphere, (ii) for stratospheric background aerosol conditions, (iii) for moderate volcanic aerosol, and (iv) for extreme volcanic aerosols. It was found that the modeled vertical color index gradients never exceed—for the 15–30-km altitude range—values of 1.05 for case (i), 1.1 for case (ii), 1.16 for case (iii), and 1.55 for case (iv). The threshold employed for the PSC detection, guided by the radiative transfer calculations, was chosen to be 1.3. Note that the PSC detection is therefore biased toward optically thicker clouds, as thin clouds below a certain slant optical thickness will fall below the threshold. Furthermore, in order to avoid false PSC identification due to ordinary cirrus clouds, it was required that the signature in the color index ratios $R_c(TH)/R_c(TH + \Delta TH)$ has to occur at least 3 km above the tropopause heights taken from Randel et al. (2000). A priori knowledge of the stratospheric aerosol loading is required as well since a massive volcanic eruption may lead to false PSC identifications if the color index gradient threshold is not adjusted accordingly.

It has to be kept in mind that PSCs can only be detected on the sunlit part of the globe using limb-scattering observations. Further investigations are in preparation to estimate the efficiency to distinguish between the different PSC types.

4. Results

a. Geographical coverage

During the Antarctic winter of 2002, SCIAMACHY was in the commissioning phase, lasting about 6 months after the successful launch of *ENVISAT*. The main emphasis during the commissioning phase was on testing and validating SCIAMACHY operations and data delivery and validating scientific data. Due to the limited SCIAMACHY data distribution during this period, only a subset of all SCIAMACHY limb-scattering ob-

servations has been available for scientific data analysis. Up to 10 (but generally less) out of 14 orbits were available as level-0 data (uncalibrated spectral data), out of which one or two orbits were calibrated to obtain level-1 spectral data. Ozone and PSC retrievals were applied to level-0 data while NO_2 and BrO retrieval required level-1 data. The fairly limited SCIAMACHY limb dataset (level 0 and level 1) available to date explains the limited spatial and temporal coverage of the limb retrieval results presented here. Limb scatter observations were all limited to the sunlit part of the polar region. Note, that the latitudinal coverage of the NO_2 retrievals in some cases extends to higher southern latitudes compared to the O_3 retrievals (e.g., in Fig. 5) since the radiative transfer model used to retrieve NO_2 profiles is more accurate at large solar zenith angles.

In this paper, we concentrated our trace gas and PSC retrievals on three selected days for which level-0 data for several consecutive orbits were available in order to highlight the effect of the peculiar meteorology on the vertical trace gas distributions. The selected days were 12 September about a week before the sudden warming, 27 September about 1 week after the start of the sudden warming and at a time when the polar vortex had established two separate centers at certain altitudes, and 2 October when one part of the polar vortex regained strength and its center position was moving back to the pole.

Meteorological data [temperature and potential vorticity (PV)] from the U.K. Met Office (UKMO) have been used for interpretation of the trace gas measurements (Swinbank and O'Neill 1994).

b. One week before the major warming: 12 September 2002

In Fig. 4, the ozone distributions at the 18-, 22-, and 26-km altitudes are shown along with the GOME total ozone distribution. The SCIAMACHY limb swaths for each limb observation are superimposed on the GOME total ozone map. In the SCIAMACHY maps, the polar vortex is indicated by the dashed modified PV contours. Here the modified PV definition referenced to the 475-K potential temperature level is used (Lait 1994). The vortex edge is characterized by maximum PV gradients, which are usually found near 40 modified potential vorticity units (MPVU). On this day the polar vortex was vertically aligned at all three altitudes. Minimum ozone is observed at all three altitudes within the confines of the polar vortex. Stratospheric temperatures are well below 195 K, the approximate upper temperature limit for potential PSC existence (also depending on the HNO_3 and H_2O abundances), for an extended region inside the polar vortex. PSC sightings by SCIAMACHY as derived from the color index (see section 3c) are indicated by small circles, and the majority of them is located in the area with temperatures below 188 K (approximate upper limit for PSC Type-2

formation). At both 18 and 22 km, PSCs were identified, while at 26 km, no PSCs were observed by SCIAMACHY. This is in line with the observation that PSCs rarely extend to altitudes above a 22-km altitude in late winter above Antarctica (Fromm et al. 1997).

In Fig. 5, latitude–altitude cross sections for ozone and NO_2 are shown along *ENVISAT* orbit 2795 crossing the 0° longitude circle at a latitude of about 60°S. This specific orbit is drawn in the ozone layer maps of Fig. 4. The MPV contour approximately delineating the vertical structure (~40 PVU, where 1 PVU = 1.0×10^{-6} m^2 s^{-1} K kg^{-1}) of the polar vortex is also depicted. Across the polar vortex edge ozone number density drops from 4×10^{12} molecules (mol) cm^{-3} (<40 PVU) to values below 2×10^{12} mol cm^{-3} well inside the polar vortex between 20 and 25 km altitude. Low NO_2 inside the polar vortex indicates strong denoxification as a most likely consequence of a combination of two processes: First, denitrification and dehydration inside the polar vortex through sedimentation of PSC particles effectively removing HNO_3, a photochemical source (Waibel et al. 1999) and second, polar night gas phase conversion into dinitrogenpentoxide (Lary et al. 1994). The first process is usually responsible for the slow-down of chlorine deactivation by conversion of active chlorine into chlorine nitrate in early spring and explains the prolonged ozone loss observed in early spring in many Arctic polar winters (Rex et al. 1997; Kleinböhl et al. 2002). Active chlorine maintained by PSC or sulphate aerosol (heterogeneous) processing at sufficiently low temperatures in combination with sunlight is responsible for the massive ozone loss extending well into spring as observed inside the Antarctic vortex (Portman et al. 1996; Brasseur et al. 1997; Solomon et al. 1999; WMO 2003).

c. The ozone "hole" split: 27 September 2002

The evolution of the polar vortex changed dramatically on 27 September as shown in Fig. 6. As indicated by the modified PV contour, the polar vortex and the polar ozone minimum region has split into two parts above about 24 km. At lower altitudes the two vortex centers appear still connected. This is also supported by the SCIAMACHY observation of a low ozone region elongated across the southern Atlantic sector of Antarctica at 18-km altitude. While minimum polar vortex ozone remained unchanged at 18 km between 12 and 27 September, an increase in the minimum ozone is observed by SCIAMACHY at 22 and 26 km. The finding that the minimum polar vortex ozone did not increase at 18 km is consistent with the POAM III O_3 measurements performed during the vortex split (Hoppel et al. 2003), which indicated only a small increase of O_3 mixing ratios within the vortex at and below the 500-K potential temperature level. Unfortunately, there are only very few POAM III measurements within the vortex at higher potential temperatures (Hoppel et al.

a)

SCIAMACHY Ozone [10^{12} mol/cm^3]: 2002/09/12

18 km

b)

SCIAMACHY Ozone [10^{12} mol/cm^3]: 2002/09/12

22 km

c)

SCIAMACHY Ozone [10^{12} mol/cm^3]: 2002/09/12
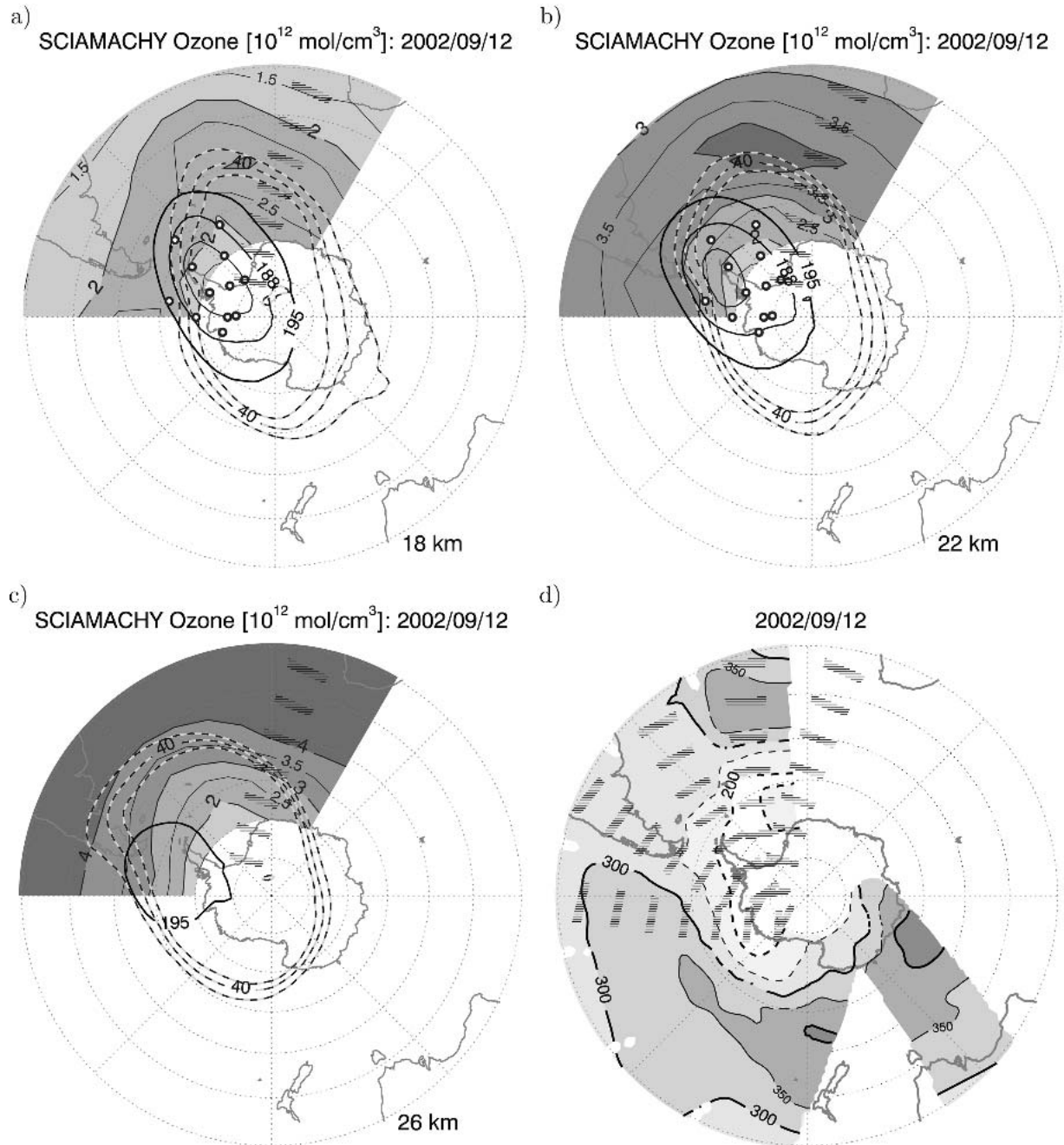
26 km

d)

2002/09/12

FIG. 4. Altitude slices through the ozone density field are shown at (a) 18, (b) 22, and (c) 26 km. The black striped rectangles indicate the locations of SCIAMACHY limb measurements for orbit 02795 (see Fig. 5). Also shown (dashed lines) are the 30, 40, and 50 MPVU [1 MPVU corresponds to 1×10^{-6} m^2 s^{-1} K kg^{-1}] contours of MPV at the corresponding altitudes. The black solid lines are isotherms at 195 (thick line), 188 (thin line), and 183 K (thinnest line). The circles within the 195-K contour in (a) and (b) indicate the locations of detected PSCs. (d)The GOME total ozone column field (in DU) together with the locations of the SCIAMACHY limb swaths (black boxes) for the orbits used here.

2003; Fig. 1), so the increased O$_3$ levels within the vortex seen in the SCIAMACHY retrievals at 22 km and above cannot be confirmed with POAM III O$_3$ measurements.

The high degree of dynamical activity has not only perturbed the vertical vortex structure but also split the minimum temperature region at all three altitudes. Because of the strong warming the area of the PSC temperature region ($T \leq 195$ K) has significantly decreased. On 27 September and also on 2 October no PSCs were

a)

Temperature and PV field along orbit 2795 on 12-SEP-2002

b)

SCIAMACHY O$_3$ retrieval, Orbit 2795, 12-SEP-2002

c)

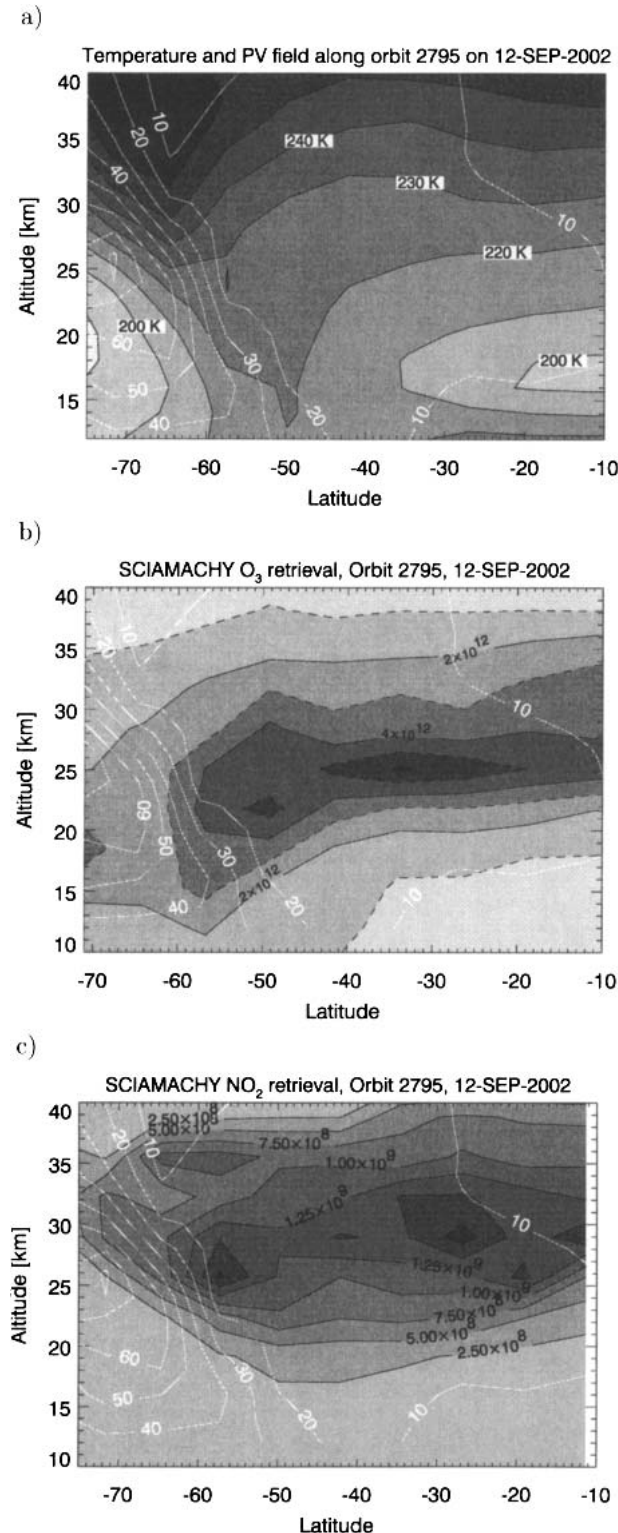SCIAMACHY NO$_2$ retrieval, Orbit 2795, 12-SEP-2002

FIG. 5. (a) Cross section through the kinetic temperature field along orbit 02795 on 12 Sep 2002. Contours of the MPV field (in MPVU) are superimposed on the temperature field. (b) The ozone density field (cm^{-3}) and (c) the NO$_2$ density field (cm^{-3}) along orbit 02795 on 12 Sep 2002. Contours of MPV are superimposed on the number density fields.

detected by SCIAMACHY, confirming the strong decline in PSCs and complete absence of ice PSC after the major warming event as observed by POAM III (Nedoluha et al. 2003).

In Fig. 7, latitude–altitude charts of ozone, NO$_2$, and temperature following the orbit near 60°E are shown. A distinct layering of alternating NO$_2$-rich and NO$_2$-poor air masses is observed near 70°S. At about 30-km altitude enhanced NO$_2$ is observed right above the lower-stratospheric polar vortex, where low NO$_2$ coincides with the minimum temperature region at 70°S near 20-km altitude. The low-ozone region inside the polar vortex in Fig. 7 appears less perturbed than nitrogen dioxide, but a vertical tilt toward the equator is observed.

Figure 6 clearly shows that the outer boundary of the polar vortex (at 22 km) and the two vortices (at 26 km), respectively, is rotated westward as one goes from 22 to 26 km. Furthermore, the vortex edges extend to lower latitudes at an altitude of 26 km compared to 22 km. This is a typical pattern of most NH major warmings with the exception that the splitting stopped here below about 24 km (Allen et al. 2003; Manney et al. 2005). The second vortex center as observed at 26 km in the southern Pacific region shows minimum ozone ($\sim 2.6 \times 10^{12}$ mol cm^{-3}), which is about 0.5×10^{12} mol cm^{-3} higher than in the first part. The rapid ozone filling in this part of the vortex remnant becomes evident about five days later as it dissipates into the midlatitude southern Pacific region, as shown in Fig. 9.

The enhanced NO$_2$ concentrations at the highest latitudes covered in orbit 3008 are consistent with GOME observations of enhanced vertical NO$_2$ columns in the same area (Richter et al. 2005). As can be seen in Fig. 7, the NO$_2$ concentrations within the enhancement are not significantly larger than the midlatitude values. Therefore, the NO$_2$ enhancement could be due to transport of midlatitude air to polar latitudes during the vortex split, as is also the case for O$_3$ (Hoppel et al. 2003). This is in line with Odin/submillimeter and millimeter radiometer (SMR) observations of N$_2$O-rich air above a layer of N$_2$O-poor vortex air, indicating the presence of midlatitude air at about 30 km (P. Ricaud 2003, personal communication), the altitude where the enhanced NO$_2$ concentrations occur. Extreme and localized enhancements (with total vertical NO$_2$ columns of up to 7×10^{13} mol cm^{-2}) of stratospheric NO$_2$ columns at polar latitudes are often associated with the final stratospheric warming usually occurring in late November and are thought to arise from photolytic conversion of reservoir of species—transported from midlatitude to polar latitudes—to NO$_x$ due to the continuous solar illumination at polar latitudes (e.g., Richter et al. 2005). To what extent this mechanism is responsible for the NO$_2$ enhancement observed by SCIAMACHY, GOME, and also OSIRIS (E. J. Llewellyn 2003, personal communication) can only be evaluated with detailed model studies.

a)

SCIAMACHY Ozone [10^{12} mol/cm^3]: 2002/09/27

18 km

b)

SCIAMACHY Ozone [10^{12} mol/cm^3]: 2002/09/27

22 km

c)

SCIAMACHY Ozone [10^{12} mol/cm^3]: 2002/09/27
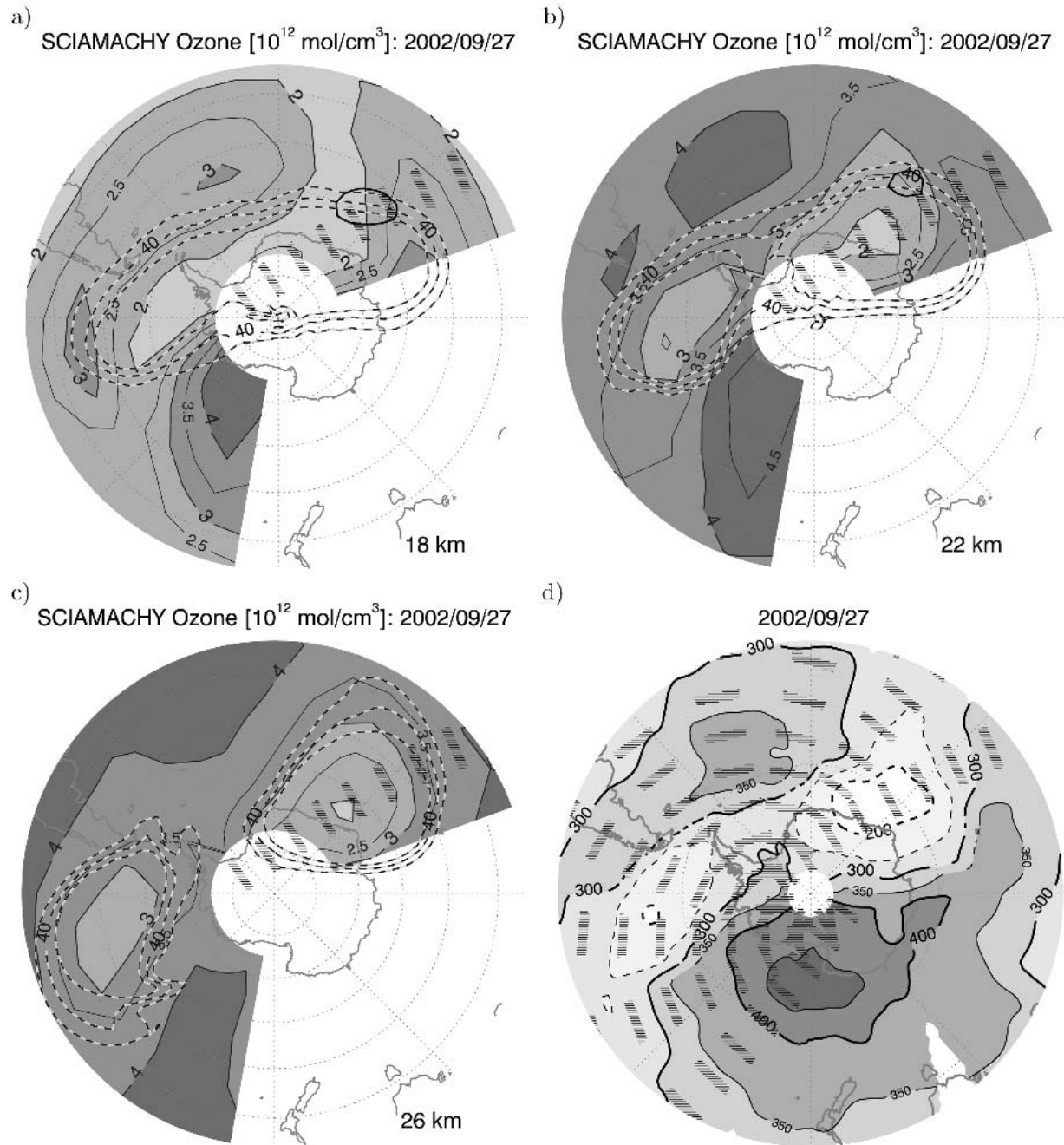

26 km

d)

2002/09/27

FIG. 6. As in Fig. 4 except for 27 Sep 2002.

Figure 8 shows a latitude–altitude cross section of the BrO mixing ratio, retrieved from SCIAMACHY measurements along orbit 3008 on 27 September. While at low and midlatitudes BrO mixing ratios are around 10 pptv; much higher BrO mixing ratios are observed inside the ozone hole area with values between about 14 and 19 pptv. The enhanced BrO there is likely to be the result of two effects: First, inorganic bromine is higher inside the lower-stratospheric polar vortex than outside due to the older age of air inside the vortex as a result of increased subsidence and confinement of air. Second, according to our current understanding of the stratospheric bromine chemistry, BrO is to a large extent controlled by NO_2 concentrations. Under normal conditions during daytime inorganic bromine will be predominantly partitioned between BrO and $BrONO_2$,
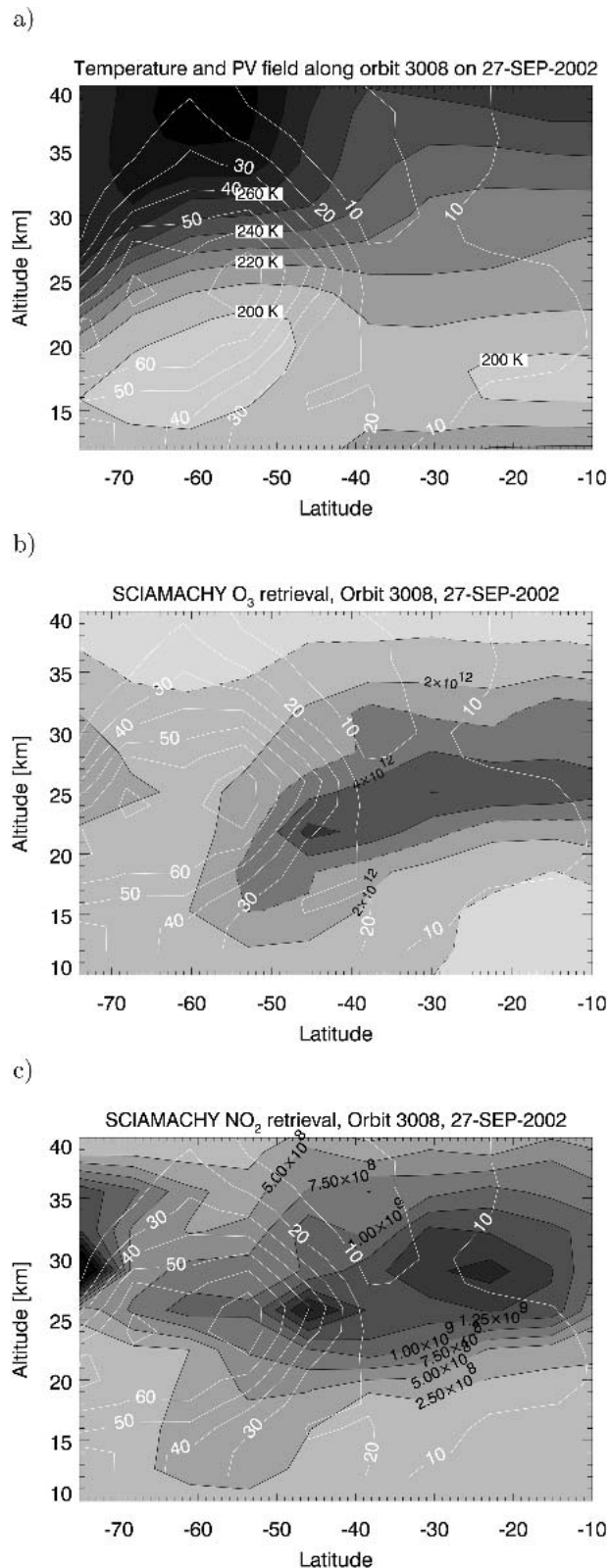
a)

b)

c)

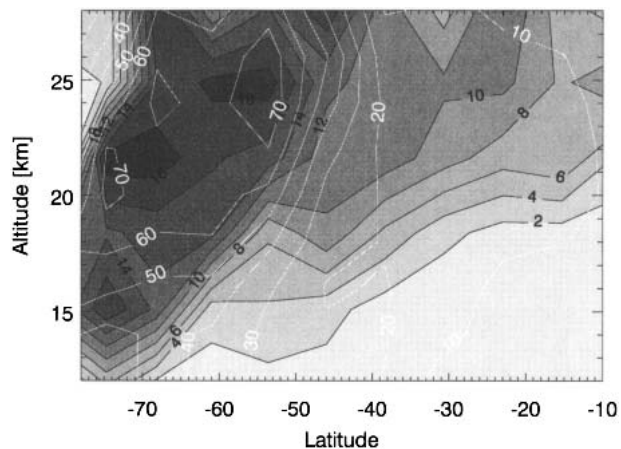FIG. 7. As in Fig. 5 except for 27 Sep 2002.

FIG. 8. Cross section of the BrO mixing ratio (in pptv) along orbit 3008 on 27 Sep 2002, retrieved from SCIAMACHY measurements. Contours of MPV are superimposed.

which is formed by the reaction of BrO with NO_2. Under ozone hole conditions, however, with very low NO_2 and enhanced ClO concentrations, $BrONO_2$ concentrations are low and inorganic bromine is expected to be partitioned predominantly between BrO and BrCl (e.g., Sinnhuber et al. 2002, and references therein). The observed BrO mixing ratios (Fig. 8) correspond to roughly 50% of the inorganic bromine outside the vortex and between about 70% and 85% inside the polar vortex, if we assume a stratospheric bromine loading of 20 to 22 pptv (e.g., Pfeilsticker et al. 2000; Sinnhuber et al. 2002). A more detailed analysis of the SCIAMACHY BrO measurements is currently being performed and will be presented elsewhere.

d. Two weeks after the major warming: 2 October 2002

The eastern part of the split vortex in the 0°–90°E sector returned closer to the pole after an additional five days, as plotted in Fig. 9. Some strong filamentation in ozone and, particularly, in the MPV contour toward South America is observed at lower altitudes (18 and 22 km). Minimum temperatures have now risen above 195 K at all altitudes. Again minimum vortex ozone remained almost unchanged at 18-km altitude; at higher altitudes minimum ozone increased, particularly above 26-km (~60%).

As shown in the latitude–altitude chart (Fig. 10), the increase of ozone at higher altitudes (26–30 km) is clearly seen. Except for a denoxified and possibly denitrified region between 15 and 20 km, rapid NO_2 increase is observed at higher altitudes in Fig. 10.

5. Discussion and conclusions

SCIAMACHY observations of ozone, NO_2, and PSCs provide important insight into the evolution of

a)

SCIAMACHY Ozone [10^{12} mol/cm^3]: 2002/10/02

18 km

b)

SCIAMACHY Ozone [10^{12} mol/cm^3]: 2002/10/02

22 km

c)

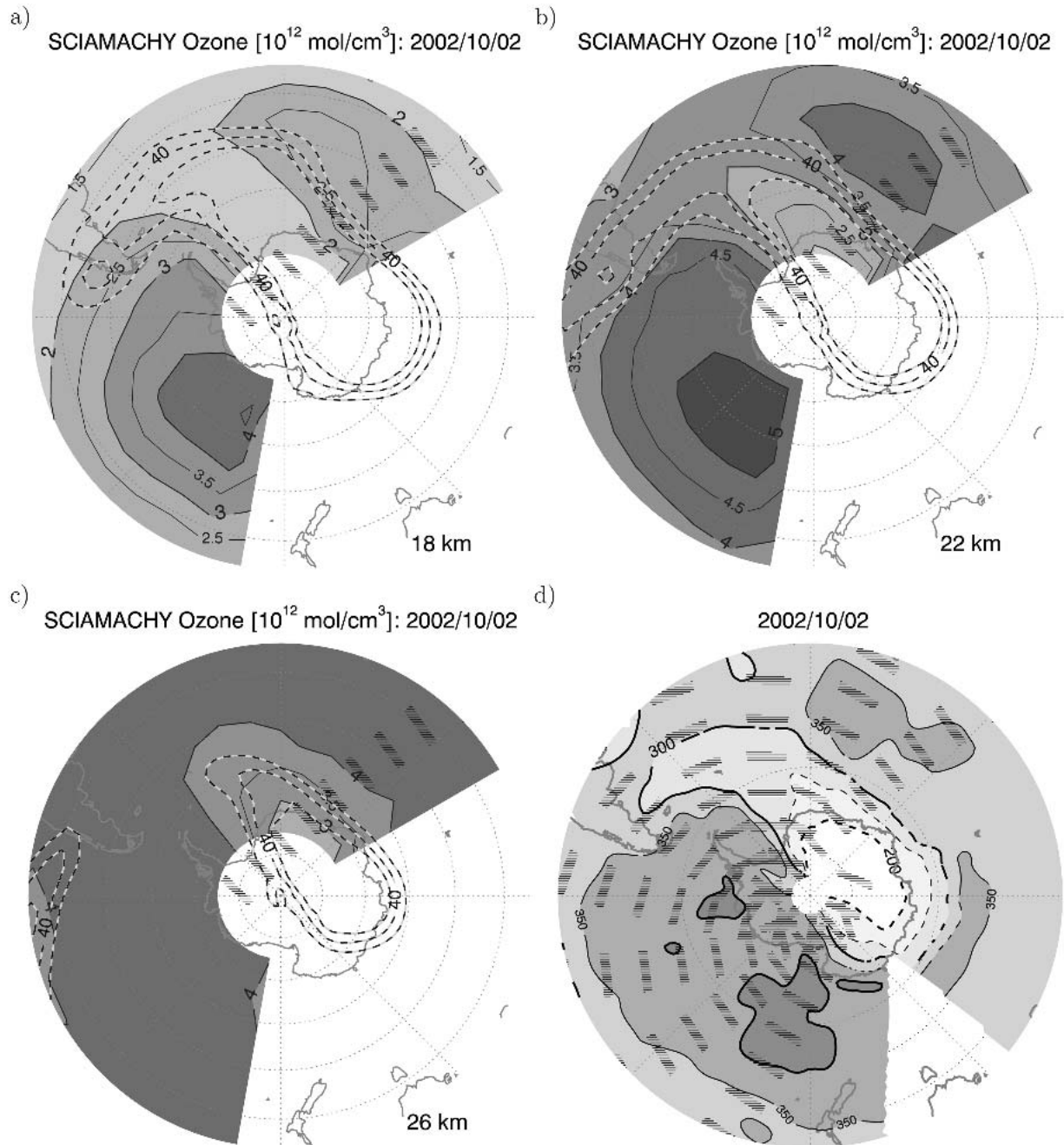SCIAMACHY Ozone [10^{12} mol/cm^3]: 2002/10/02

26 km

d)

2002/10/02

FIG. 9. As in Fig. 4 except for 2 Oct 2002.

the Antarctic vortex during an unprecedented SH major warming event. A series of strong minor warmings in the mid stratosphere were observed throughout the winter starting in May (Sinnhuber et al. 2003; Allen et al. 2003). This did not, however, strongly affect the lower-stratospheric temperatures. Minimum temperatures at 46 hPa were in the usual range observed in earlier winters, but an unusually rapid increase above 195 K occurred on 29 September according to UKMO.

Within the last 10 years such a rise is usually observed about four weeks later, for example, on 18 October in 2000 and on 25 October in 2001. This early rise was related to the midstratospheric major warming initiated almost instantaneously by the extreme eddy heat flux through the 100-hPa level observed on 21 and 22 September at 43°–70°S (Sinnhuber et al. 2003), guiding unusually high wave energy into the stratosphere. The perturbation was sufficiently large to warm the strato-

a)

Temperature and PV field along orbit 3080 on 02-OCT-2002

b)

SCIAMACHY O$_3$ retrieval, Orbit 3080, 02-OCT-2002

c)

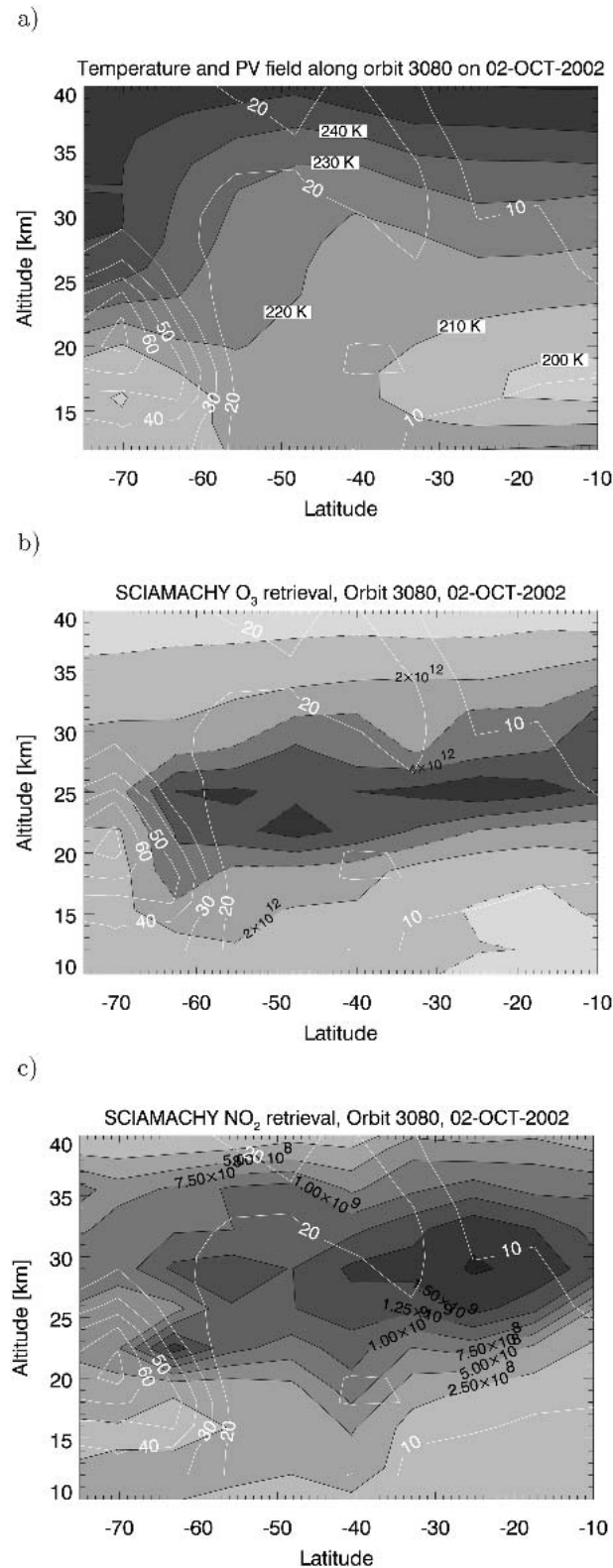SCIAMACHY NO$_2$ retrieval, Orbit 3080, 02-OCT-2002

FIG. 10. As in Fig. 5 except for 2 Oct 2002.

sphere from the mid stratosphere down to the lower stratosphere and strongly perturb stratospheric circulation.

Ozone observations confirm the vertical integrity of the lower-stratospheric vortex just before the onset of the major warming as shown in the SCIAMACHY ozone maps at 18, 22, and 26 km altitude on 12 September (Fig. 4). Extensive areas of PSCs (mostly within the 188-K contour) were observed by SCIAMACHY up to about 23–24-km.

After the major warming no PSCs were observed by SCIAMACHY (27 September and 2 October). On 27 September the ozone minima on the SCIAMACHY altitude maps show—like the GOME total ozone map—a split at 26 km and above, while at 18 km the low ozone area appears elongated and shifted to the South Atlantic sector. A westward and equatorward tilt with altitude can be seen in the SCIAMACHY minimum ozone. This is a vortex pattern that has been observed in many NH major warmings (Manney et al. 2005). At 26-km altitude the vortex remnant in the western sector dissipated quickly into lower southern latitudes in the Pacific region. Rapid ozone increase was observed in this remnant and may indicate efficient mixing with midlatitude air. The other part of the vortex restabilized and moved closer to the pole on 2 October.

At 18-km altitude minimum ozone remained unchanged during the period investigated here. Strong filamentation was evident in the MPV data rather than a vortex split. At higher altitudes an increase in ozone number density inside the remaining polar vortex is observed until 2 October. The ozone number density has risen by about 60% up to that day. The reestablishment of the polar vortex in the lowermost stratosphere is confirmed by the SCIAMACHY observations. In line with POAM III observations (Hoppel et al. 2003; Allen et al. 2003), the upper lower stratosphere and mid stratosphere remained strongly perturbed. Rapid NO$_2$ recovery at altitudes above 25 km was observed by SCIAMACHY, and only a small region with denoxified and possibly denitrified air remained below 20-km. In conclusion, SCIAMACHY limb observations of stratospheric minor constituent profiles with their near-global coverage and high vertical resolution can provide important information on the evolution of the Antarctic stratosphere during the major warming in September 2002 and stratospheric processes in general.

REFERENCES

Allen, D. R., R. M. Bevilaqua, G. E. Nedoluha, C. E. Randall, and G. L. Manney, 2003: Unusual stratospheric transport and mixing during the 2002 Antarctic winter. *Geophys. Res. Lett.,* **30,** 1599, doi:10.1029/2003GL017117.

Baldwin, M., T. Hirooka, A. O'Neill, and S. Yoden, 2003: Major stratospheric warming in the Southern Hemisphere in 2002: Dynamical aspects of the ozone hole split. *SPARC Newsletter,* No. 20, SPARC Office, Toronto, ON, Canada, 24–26.

Bovensmann, H., J. P. Burrows, M. Buchwitz, J. Frerick, S. Noël, V. V. Rozanov, K. V. Chance, and A. P. G. Goede, 1999: SCIAMACHY: Mission objectives and measurement modes. *J. Atmos. Sci.,* **56,** 127–150.

Bracher, A., M. Weber, K. Bramstedt, A. Richter, and A. Rozanov, C. von Savigny, M. von König, and J. P. Burrows, 2002: Validation of ENVISAT trace gas data products by comparison with GOME/ERS-2 and other satellite sensors. *Proc. of the ENVISAT Validation Workshop,* SP-531, Frascati, Italy, ESA, CD-ROM.

——, A. Rozanov, C. von Savigny, M. von König, M. Weber, K. Bramstedt, and J. P. Burrows, 2003: First validation of SCIAMACHY O_3 and NO_2 profiles with collocated measurements from satellite sensors HALOE, SAGE II and POAM III. *Geophysical Research Abstracts,* Vol. 5, EGU, 08793.

Brasseur, G. P., X. Te, P. J. Rasch, and F. Lefévre, 1997: A three-dimensional simulation of the Antarctic ozone hole: Impact of anthropogenic chlorine on the lower stratosphere and upper troposphere. *J. Geophys. Res.,* **102** (D7), 8909–8930.

Burrows, J. P., M. Weber, M. Buchwitz, V. V. Rozanov, A. Ladstätter, M. Eisinger, and D. Perner, 1999: The Global Ozone Monitoring Experiment (GOME): Mission concept and first scientific results. *J. Atmos. Sci.,* **56,** 151–175.

Eichmann, K.-U., J. Kaiser, C. von Savigny, A. Rozanov, V. V. Rozanov, H. Bovensmann, M. von König, and J. P. Burrows, 2003: SCIAMACHY limb measurements in the UV/vis spectral region: First results. *Adv. Space Res.,* **34,** 775–779.

Fischer, H., and H. Oelhaf, 1996: Remote sensing of vertical profiles of atmospheric trace constituents with MIPAS limb emission spectrometers. *Appl. Opt.,* **35,** 2787–2796.

Flittner, D. E., P. K. Bhartia, and B. M. Herman, 2000: O_3 profiles retrieved from limb scatter measurements: Theory. *Geophys. Res. Lett.,* **27,** 2061–2064.

Fromm, M. D., J. D. Lumpe, R. M. Bevilacqua, E. P. Shettle, J. Hornstein, S. T. Massie, and K. H. Fricke, 1997: Observations of Antarctic polar stratospheric clouds by POAM II: 1994–1996. *J. Geophys. Res.,* **102,** 23 659–23 672.

Griffioen, E., and L. Oikarinen, 2000: LIMBTRAN: A pseudo three-dimensional radiative transfer model for the limb-viewing imager OSIRIS on the ODIN satellite. *J. Geophys. Res.,* **105** (D24), 29 717–29 730.

Haley, C. S., C. von Savigny, C. E. Sioris, I. C. McDade, E. Griffioen, E. J. Llewellyn, and D. P. Murtagh, 2003: A comparison of two methods to retrieve stratospheric O_3 profiles from Odin/OSIRIS observations of limb radiance spectra. *Adv. Space Res.,* **34,** 769–774.

Hoogen, R., V. V. Rozanov, and J. P. Burrows, 1999: Ozone profiles from GOME satellite data: Algorithm description and first validation. *J. Geophys. Res.,* **104,** 8263–8280.

Hoppel, K., R. Bevilaqua, D. Allen, G. Nedoluha, and C. Randall, 2003: POAM III observations of the anomalous 2002 Antarctic ozone hole. *Geophys. Res. Lett.,* **30,** 1394, doi:10.1029/2003GL016899.

Kaiser, J. W., 2002: *Atmospheric Parameter Retrieval from UV-vis-NIR Limb Scattering Measurements.* Logos Verlag, 300 pp.

——, and J. P. Burrows, 2003: Fast weighting functions for retrievals from limb scattering measurements. *J. Quant. Spectrosc. Radiat. Transfer,* **77,** 273–283.

Kleinböhl, A., and Coauthors, 2002: Vortexwide denitrification of the Arctic polar stratosphere in winter 1999/2000 determined by remote observations. *J. Geophys. Res.,* **107,** 8305, doi:10.1029/2001JD001042.

Lait, L. R., 1994: An alternative form for potential vorticity. *J. Atmos. Sci.,* **51,** 1754–1759.

Lary, D. J., J. A. Pyle, and G. Carver, 1994: A three-dimensional model study of nitrogen oxides in the stratosphere. *Quart. J. Roy. Meteor. Soc.,* **120,** 453–482.

Llewellyn, E. J., and Coauthors, 1997: OSIRIS—An application of tomography for absorbed emissions in remote sensing. *Applications of Photonic Technology 2,* G. A. Lampropoulos and R. A. Lessard, Eds., Plenum Press, 627–632.

Lucke, R. L., and Coauthors, 1999: The Polar Ozone and Aerosol Measurement (POAM) III instrument and early validation results. *J. Geophys. Res.,* **104,** 18 785–18 799.

Manney, G. L., and Coauthors, 2005: Simulations of dynamics and transport during the September 2002 Antarctic major warming. *J. Atmos. Sci.,* **62,** 690–707.

McCormick, M. P., J. M. Zawodny, R. E. Veiga, J. C. Larsen, and P. H. Wang, 1989: An Overview of SAGE I and II Ozone Measurements. *Planet. Space Sci.,* **37,** 1567–1586.

McPeters, R. D., P. K. Bhartia, A. J. Krueger, and J. R. Herman, 1998: Earth probe Total Ozone Mapping Spectrometer (TOMS) data product user's guide. Tech. Rep. NASA/IP-1998-206895, 60 pp.

——, S. J. Janz, E. Hilsenrath, and T. L. Brown, 2000: The retrieval of O_3 profiles from limb scatter measurements: Results from the Shuttle Ozone Limb Sounding Experiment. *Geophys. Res. Lett.,* **27,** 2601–2604.

Nedoluha, G. E., R. M. Bevilacqua, M. D. Fromm, K. W. Hoppel, and D. R. Allen, 2003: POAM measurements of PSCs and water vapor in the 2002 Antarctic vortex. *Geophys. Res. Lett.,* **30,** 1796, doi:10.1029/2003GL017577.

Newman, P. A., and E. R. Nash, 2005: The unusual Southern Hemisphere stratosphere winter of 2002. *J. Atmos. Sci.,* **62,** 614–628.

Petelina, S. V., and Coauthors, 2004: Comparison of the OSIRIS/Odin stratospheric ozone profiles with coincident POAM III sonde measurements. *Geophys. Res. Lett.,* **31,** L07104, doi:10.1029/2003GL019299.

Pfeilsticker, K., and Coauthors, 2000: Lower stratospheric organic and inorganic bromine budget for the Arctic winter 1998/99. *Geophys. Res. Lett.,* **27,** 3305–3308.

Portmann, R. W., S. Solomon, R. R. Garcia, L. W. Thomason, L. R. Poole, and M. P. McCormick, 1996: Role of aerosol variations in anthropogenic ozone depletion in the polar region. *J. Geophys. Res.,* **101** (D17), 22 991–23 006.

Randel, W. J., W. Wu, and D. Gaffen, 2000: Interannual variability of the tropical tropopause derived from radiosonde data and NCEP reanalyses. *J. Geophys. Res.,* **105,** 15 509–15 523.

Rex, M., and Coauthors, 1997: Prolonged stratospheric ozone loss in the 1995/1996 Arctic winter. *Nature,* **389,** 835–838.

Richter, A., and Coauthors, 2005: GOME observations of stratospheric trace gas distributions during the splitting vortex event in the Antarctic winter of 2002. Part I: Measurements. *J. Atmos. Sci.,* **62,** 778–785.

Rodgers, C. D., 1976: Retrieval of atmospheric temperature and

composition from remote measurements of thermal radiation. *Rev. Geophys. Space Phys.,* **14,** 609–624.

——, 1990: Characterization and error analysis of profiles retrieved from remote sounding measurements. *J. Geophys. Res.,* **95,** 5587–5595.

Roscoe, H. K., J. D. Shanklin, and S. R. Colwell, 2005: Has the Antarctic vortex split before 2002? *J. Atmos. Sci.,* **62,** 581–588.

Rozanov, A., V. Rozanov, and J. P. Burrows, 2001: A numerical radiative transfer model for a spherical planetary atmosphere: Combined differential-integral approach involving the Picard iterative approximation. *J. Quant. Spectrosc. Radiat. Transfer,* **69,** 513–534.

Sarkissian, A., J.-P. Pommereau, and F. Goutail, 1994: PSC and volcanic aerosol observations during EASOE by UV–visible ground-based spectrometry. *Geophys. Res. Lett.,* **21,** 1319–1322.

Sinnhuber, B.-M., and Coauthors, 2002: Comparison of measurements and model calculations of stratospheric bromine monoxide. *J. Geophys. Res.,* **107,** 4398, doi:10.1029/2001JD000940.

——, M. Weber, A. Amankwah, and J. P. Burrows, 2003: Total ozone during the unusual Antarctic winter of 2002. *Geophys. Res. Lett.,* **30,** 1580, doi:10.1029/2002GL016798.

Sioris, C., C. von Savigny, R. L. Gattinger, J. C. McConnell, I. C. McDade, E. Griffioen, E. J. Llewellyn, and the ODIN team, 2001: Attitude Determination for Limb-Scanning Satellites: The "knee at 305 nm. *Eos, Trans. Amer. Geophys. Union,* **82** (Suppl.), A32B-0056.

——, and Coauthors, 2003: Stratospheric profiles of nitrogen dioxide observed by OSIRIS on the Odin satellite. *J. Geophys. Res.,* **108,** 4215, doi:10.1029/2002JD002672.

Solomon, S., 1999: Stratospheric ozone depletion: A review of concepts and history. *Rev. Geophys.,* **37,** 275–316.

Stolarski, R. S., R. D. McPeters, and P. A. Newman, 2005: The ozone hole of 2002 as measured by TOMS. *J. Atmos. Sci.,* **62,** 716–720.

Swinbank, R., and A. O'Neill, 1994: A stratosphere–troposphere data assimilation system. *Mon. Wea. Rev.,* **122,** 686–702.

Varotsos, C., 2002: The Southern Hemisphere ozone hole split in 2002. *Environ. Sci. Pollut. Res.,* **9,** 375–376.

von Clarmann, T., and Coauthors, 2003: Retrieval of temperature and tangent altitude pointing from limb emission spectra recorded from space by the Michelson interferometer for passive atmospheric sounding. *J. Geophys. Res.,* **108,** 4736, doi:10.1029/2003JD003602.

von Savigny, C., and Coauthors, 2003: Stratospheric ozone profiles retrieved from limb scattered sunlight radiance spectra measured by the OSIRIS instrument on the Odin satellite. *Geophys. Res. Lett.,* **30,** 1755, doi:10.1029/2002GL016401.

Vountas, M., V. V. Rozanov, and J. P. Burrows, 1998: Ring effect: Impact of rotational Raman scattering on radiative transfer in Earth's atmosphere. *J. Quant. Spectrosc. Radiat. Transf.,* **60,** 943–961.

Waibel, A. E., and Coauthors, 1999: Arctic ozone loss due to denitrification. *Science,* **283,** 2064–2069.

Weber, M., S. Dhomse, F. Wittrock, A. Richter, B.-M. Sinnhuber, and J. P. Burrows, 2003: Dynamical control of NH and SH winter/spring total ozone from GOME observations in 1995–2002. *Geophys. Res. Lett.,* **30,** 1583, doi:10.1029/2002GL016799.

WMO, 2003: Scientific assessment of ozone depletion. 2002 Global Ozone Research and Monitoring Project Rep. 47, World Meteorological Organization, Geneva, Switzerland, 498 pp.